INTERNATIONAL JOURNAL OF INTEGRATED ENGINEERING
ISSN: 2229-838X e-ISSN: 2600-7916

IJIE

Vol. 17 No. 8 (2025) 285-300
https://publisher.uthm.edu.my/ojs/index.php/ijie

Computational Study on the Hemodynamic Analysis of Intracranial Aneurysms using Flow Diverter Stents

Muhammad Affiq Syukri Arafat[1], Nor Adrian Nor Salim[1]*, Mohd Syahar Mohd Shawal[2], Mohd Rosdzimin Abdul Rahman[3]

[1] *Department of Mechanical Engineering, Faculty of Mechanical Engineering and Manufacturing, Universiti Tun Hussein Onn Malaysia, Parit Raja, Batu Pahat, Johor, 86400, MALAYSIA*
[2] *School of Mechanical Engineering and Manufacturing, Universiti Teknologi MARA, Shah Alam, Selangor, 40450, MALAYSIA*
[3] *Department of Mechanical Engineering, Faculty of Engineering, Universiti Pertahanan Nasional Malaysia, Kem Sg. Besi, Kuala Lumpur, 57000, MALAYSIA*

*Corresponding Author: adrian@uthm.edu.my
DOI: https://doi.org/10.30880/ijie.2025.17.08.024

Article Info

Received: 12 July 2025
Accepted: 1 December 2025
Available online: 31 December 2025

Keywords

Intracranial aneurysm, flow diverter stent, computational fluid dynamics (CFD), time averaged wall shear stress, oscillatory shear index, relative residence time

Abstract

Intracranial aneurysms represent a critical cerebrovascular pathology with a high risk of rupture-induced subarachnoid haemorrhage, necessitating effective endovascular interventions such as flow diverter (FD) stents to reconstruct the parent vessel and induce curative thrombosis. However, the therapeutic efficacy of these devices varies significantly based on their geometric configuration, requiring precise analysis of the hemodynamic alterations they induce within the aneurysm sac. This study aims to perform a comprehensive computational fluid dynamics (CFD) investigation to quantify changes in velocity, time-averaged wall shear stress (TAWSS), oscillatory shear index (OSI), and relative residence time (RRT) following the virtual deployment of five distinct FD stent designs. Using ANSYS Fluent 2023, transient simulations were conducted on an idealized saccular aneurysm model under pulsatile physiological conditions, treating blood as an incompressible Newtonian fluid to compare a baseline untreated model against five stented configurations (Models 2–6). The quantitative results demonstrated that stent geometry critically influences flow diversion; specifically, Model 6 exhibited the most superior performance by achieving near-complete flow stagnation with velocity and pressure reductions exceeding 90% compared to the untreated baseline velocity of 0.39 ± 0.04 m/s, and Model 3 achieved a beneficial 5.54% reduction in WSS, whereas Model 5 proved suboptimal with a 2.77% increase in WSS and unfavourable residence time characteristics. In conclusion, the study confirms that optimizing stent design parameters is essential for establishing the low-flow, high-residence-time environment required for successful aneurysm occlusion, thereby validating CFD as a vital predictive tool for enhancing FD treatment strategies.

1. Introduction

Intracranial aneurysms (IAs), also known as a cerebral or brain aneurysm, is a condition where part of a blood vessel in the brain bulges or expands due to a weakened vessel wall. This weakening usually occurs when the

middle and inner layers of the artery are damaged, and the smooth muscle cells that maintain their strength are reduced. Depending on the shape, the aneurysm can be either saccular (sac-like) or fusiform (spindle-shaped). The wall of the aneurysm becomes thinner and less elastic, making it more likely to rupture under blood pressure. When an aneurysm ruptures, it can cause a subarachnoid hemorrhage (SAH), which is a serious and potentially fatal type of brain bleeding [1], [2]. Therefore, early detection, detailed analysis, and proper treatment of both ruptured and unruptured aneurysms are crucial. These efforts rely on modern imaging techniques, computer-based simulations, and collaboration among medical and engineering specialists [3].

Historically, treatment options included surgical clipping, but minimally invasive endovascular techniques have become the primary modality for many cases. Among these, the development of flow diverter (FD) stents has revolutionized the management of complex, wide-necked, or fusiform aneurysms. Unlike traditional coiling which aims to fill the aneurysm sac, an FD is a high-mesh-density stent deployed across the aneurysm neck in the parent artery [4]. The fundamental principle of an FD is to reconstruct the parent vessel, thereby redirecting blood flow away from the aneurysm sac. This flow diversion promotes intra-aneurysmal stasis, leading to progressive thrombosis and, ultimately, the exclusion of the aneurysm from circulation while allowing perforating vessels covered by the stent to remain patent [5], [6].

The pathogenesis of IAs and the therapeutic mechanism of FDs are intrinsically linked to cerebral hemodynamics. It is widely accepted that abnormal hemodynamic forces play a crucial role in the lifecycle of an aneurysm [7]. Factors such as high-velocity inflow jets impinging on the aneurysm wall can create regions of high wall shear stress (WSS), which may drive aneurysm growth and degradation of the vessel wall. Conversely, areas of low and swirling flow can also contribute to pathological remodelling. Therefore, the hemodynamic environment, characterized by parameters like blood velocity and intra-aneurysmal pressure, is a direct determinant of rupture risk and treatment efficacy. Analyzing these forces provides invaluable insight into both the natural history of the disease and the response to treatment [8].

Computational Fluid Dynamics (CFD) has emerged as an indispensable tool for performing detailed, patient-specific hemodynamic analyses. By creating 3D models from medical imaging data (such as 3D rotational angiography), CFD simulations can non-invasively quantify complex blood flow patterns and hemodynamic parameters that are impossible to measure directly in vivo [9]. Following the virtual deployment of an FD, CFD can predict the post-treatment hemodynamic environment, offering a powerful method to understand the device's mechanism of action. Studies have consistently demonstrated that FDs significantly reduce inflow velocity into the aneurysm sac, leading to a marked decrease in intra-aneurysmal kinetic energy and normalization of pressure gradients, which are key factors for successful occlusion [10].

Beyond basic parameters, advanced hemodynamic indices provide a more nuanced understanding of the forces acting on the vessel wall. The Oscillatory Shear Index (OSI) quantifies the directional variation of WSS throughout the cardiac cycle, with high OSI values indicating highly oscillatory flow, which is known to be pro-inflammatory and dysfunctional for endothelial cells. Similarly, the Relative Residence Time (RRT) measures the duration that blood particles remain in proximity to the vessel wall, with elevated RRT indicating areas of flow stasis. Since the therapeutic goal of an FD stent is to induce flow stasis, this study specifically monitors increases in RRT (indicating flow stagnation) and OSI (indicating unstable, non-directional flow), as high values for both indices within the aneurysm sac are strongly correlated with the desired thrombus formation and subsequent aneurysm occlusion [6], [11].

Despite the widespread clinical success of FDs, treatment outcomes can be variable, with factors like aneurysm morphology, device positioning, and individual patient hemodynamic influencing the time to occlusion and overall success rate [12]. A significant knowledge gap remains in prospectively identifying which aneurysm configurations will respond best to flow diversion. Therefore, detailed computational investigations are crucial to elucidate the precise hemodynamic changes that govern treatment success. This study aims to perform a comprehensive CFD analysis on an idealized intracranial aneurysm model, quantifying the alterations in TAWSS, velocity, pressure, OSI, and RRT before and after the virtual implantation of a flow diverter stent. The objective is to correlate these specific hemodynamic modifications with the mechanisms driving successful and timely aneurysm thrombosis.

2. Methodology

The computational investigation was conducted by modelling blood flow in a simplified intracranial aneurysm model treated with a flow diverter stent. The simulation was performed using ANSYS Fluent 2023, a CFD platform capable of examining the intricate hemodynamic behaviour inside blood vessels. This software also provides detailed information on parameters such as blood velocity, wall shear stress (WSS), and pressure, which are essential for optimising the design and effectiveness of flow diverter stents. A typical CFD study is divided into three main phases—pre-processing, solving, and post-processing [13]. The pre-processing stage focuses on preparing the model before execution. This includes constructing patient-specific aneurysm geometry, generating the mesh, setting boundary conditions, and selecting suitable physical models to represent blood flow. The solving

stage involves configuring the numerical solver, which requires choosing the solver type, applying discretization methods, defining convergence criteria, and determining time-step settings to properly capture pulsatile flow. The final stage, post-processing, is carried out once the simulation finishes. It includes validating the obtained results, evaluating the hemodynamic characteristics, producing visualizations, and compiling the findings into reports [10], [14].

2.1 Governing Equation

This study simulates fluid dynamics using the continuity and Navier-Stokes equations, which govern the motion of an incompressible fluid. These equations are essential for describing flow behaviour in complex geometries, such as those introduced by intravascular stents [15].

The numerical simulation was performed under the assumption of a laminar flow regime, which is appropriate for the low Reynolds number conditions typical of blood flow in small arteries. This allows for the direct solution of the governing equations without the need for turbulence modelling. The conservation of mass and momentum are represented by the continuity (incompressible) and Navier-Stokes equations, respectively, as formulated in Eq. (1) and Eq. (2) [16]:

$$\nabla.(\vec{v}) = 0 \tag{1}$$

$$\rho\left(\frac{\partial \vec{v}}{\partial t} + \vec{v}.\nabla\vec{v}\right) = -\nabla p + \mu\nabla^2\vec{v} + \vec{F} \tag{2}$$

Here, ρ is fluid density, v is the velocity vector, p is pressure, μ is dynamic viscosity and F represent body forces.

2.2 Hemodynamic Parameters of Intracranial Artery

Multiple hemodynamic indicators were utilized to assess how morphological variations influence the formation of atherosclerosis-prone regions in intracranial arteries.

2.2.1 Time Averaged Wall Shear Stress (TAWSS)

The hemodynamic environment of intracranial arteries is critical to their structural and functional integrity, with Time-Averaged Wall Shear Stress (TAWSS) serving as a key indicator. Wall Shear Stress (WSS), defined as the tangential frictional force exerted by blood flow on the arterial endothelium, is instrumental in predicting vascular remodelling and disease progression. The magnitude of WSS can be quantified using various formulations. Under idealized laminar flow, it is given by Poiseuille's law as written in Eq. (3), which relates WSS to blood's dynamic viscosity, μ_d, flow rate, Q and the arterial radius, r. A more general definition, applicable in complex geometries, derives WSS from the fluid viscous stress tensor (τ_{ij}) as expressed in Eq. (4) [17], [18].

$$\tau_w = \frac{4\mu_d Q}{\pi r^3} \tag{3}$$

$$\tau_w = t - (t \cdot n)n \tag{4}$$

Aberrant WSS values within the cerebral vasculature are linked to distinct pathologies. Specifically, low WSS values of less than 1 Pa promote an atherogenic endothelial phenotype, increasing susceptibility to atherosclerosis. In contrast, high WSS values exceeding 7 Pa can lead to endothelial dysfunction and a heightened risk of thrombotic events or plaque erosion. The physiological range for healthy intracranial arteries is generally accepted to be between 1 and 7 Pa. Since cerebral blood flow is inherently pulsatile, a time-averaged value is required for meaningful analysis. TAWSS is therefore computed by integrating the instantaneous WSS magnitude, $|\tau_w|$, over the period of one full cardiac cycle, T, as shown in Eq. (5) [18].

$$TAWSS = \frac{1}{T}\int_0^T |\vec{\tau}_w|\, dt \tag{5}$$

2.2.2 Oscillatory Shear Index (OSI)

The Oscillatory Shear Index (OSI) is a critical hemodynamic metric used to characterize the temporal fluctuations in the direction of shear forces acting on the walls of intracranial arteries throughout the cardiac cycle. This

parameter is instrumental in identifying locations with significant blood flow recirculation and stasis, which are implicated in cerebrovascular pathologies. The OSI, derived from the oscillatory component of wall shear stress (WSS), is a dimensionless value that ranges from 0 (indicating completely unidirectional flow) to 0.5 (representing purely oscillatory flow). In the context of intracranial hemodynamics, regions exhibiting a high OSI, specifically values greater than 0.2, are considered to be at an elevated risk for atherosclerotic plaque formation and progression. The computation of the OSI is defined by Eq. (6) as presented [19].

$$OSI = \frac{1}{2}\left(1-\frac{|\int_0^T \vec{\tau}_w dt|}{\int_0^T |\vec{\tau}_w| dt}\right) \quad (6)$$

2.2.3 Relative Residence Time (RRT)

Relative Residence Time (RRT) is a hemodynamic parameter applied to intracranial arteries to characterize the interaction between blood particles and the vessel wall. Elevated RRT values occur in regions of low and oscillatory shear stress, representing disturbed flow conditions that facilitate intracranial atherosclerosis. Prolonged particle residence enhances platelet adhesion, protein accumulation, and thrombus stabilization on the endothelium. Accordingly, RRT is a reliable predictor of arterial segments prone to atherogenesis, with values above 10 Pa^{-1} often associated with advanced disease progression. RRT is computed from time-averaged wall shear stress (TAWSS) and oscillatory shear index (OSI), as expressed in Eq. (7) [20].

$$RRT = \frac{1}{(1-2\cdot OSI)\cdot TAWSS} \quad (7)$$

2.3 Simplified Geometry Model

The three-dimensional (3D) geometry representing an idealized intracranial saccular aneurysm was developed for the present analysis. The model was initially constructed using the computer-aided design (CAD) software SolidWorks 2023 and subsequently imported into ANSYS Fluent 2023 DesignModeler for pre-processing and simulation setup [21]. The study utilized a total of six computational models to evaluate hemodynamic performance. Fig. 1 illustrates the simplified geometry of the intracranial aneurysm Model 1, including the parent artery and the saccular dome configuration used in this study. Model 1 served as the Baseline (No-Stent) Model, representing the untreated aneurysm geometry. The geometry consists of a straight parent artery, modelled as a cylinder with a uniform diameter of 4 mm and a total length of 50 mm [22]. A saccular aneurysm with a maximum dome diameter of 10 mm and a neck width of 7.55 mm is positioned on the wall of the parent vessel, reflecting a typical morphology for this type of vascular condition [23].

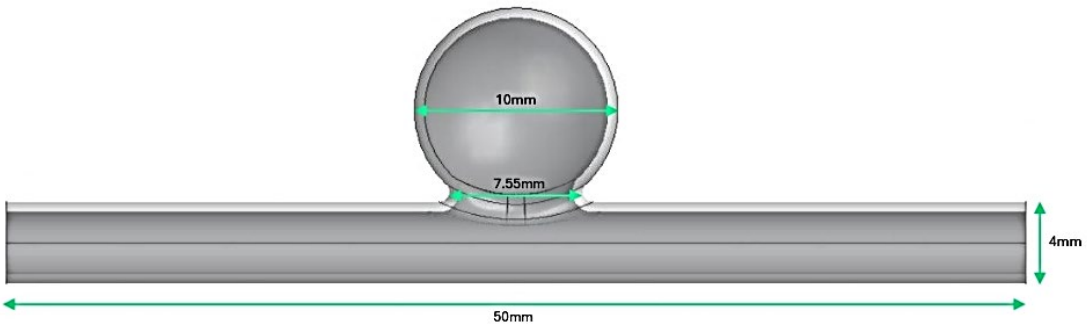

Fig. 1 *Geometry of simplified intracranial aneurysms model (Model 1)*

During the simulation phase, each of the five stent geometries was virtually deployed within the idealized aneurysm model. As shown in Fig. 2, the stents were strategically positioned to span the 7.55 mm neck width. This arrangement replicates the clinical procedure where the stent acts as a scaffold to divert blood flow away from the aneurysm sac [24]. By maintaining a constant aneurysm and parent vessel morphology across all six simulations (1 Baseline + 5 Stented), any variations in hemodynamic parameters can be directly attributed to the stent design. This process produced five complete computational models, labelled (a) through (e) in Fig. 3. Each model included the parent artery, the saccular aneurysm, and one of the five implanted stent designs. By maintaining a constant aneurysm and parent vessel morphology across all simulations, any variations in hemodynamic parameters such as intra-aneurysmal flow velocity, pressure distribution, and wall shear stress can be directly attributed to the geometric design of the stent. This ensures a rigorous and unbiased assessment of each stent's therapeutic performance [25].

Int. Journal of Integrated Engineering Vol. 17 No. 8 (2025) p. 285-300

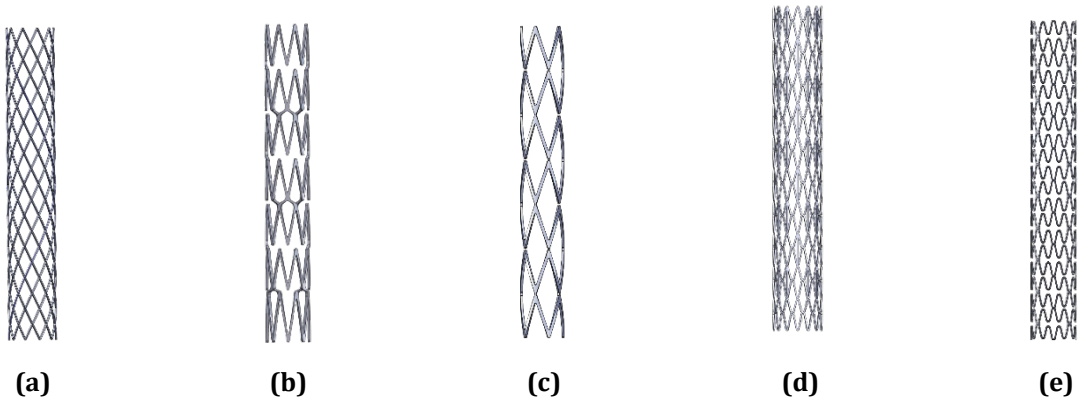

Fig. 2 *Geometry for 5 types of stents (a) Type 1; (b) Type 2; (c) Type 3; (d) Type 4; (e) Type 5*

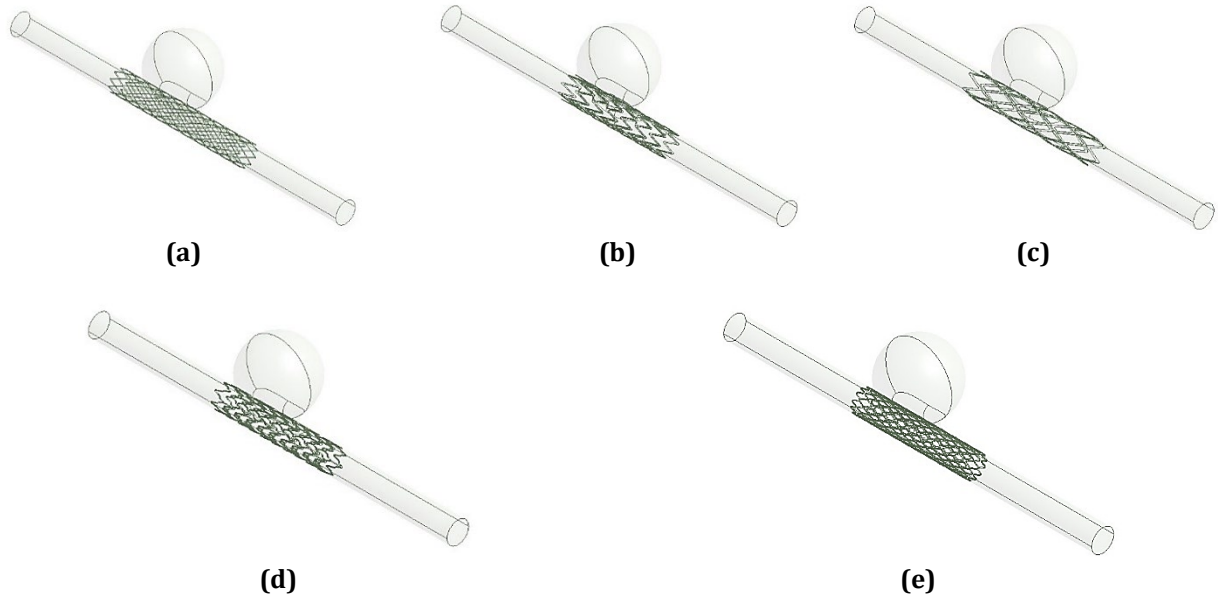

Fig. 3 *Simulation geometry for the five stent-aneurysm configurations (a) Model 2; (b) Model 3; (c) Model 4; (d) Model 5; (e) Model 6*

Table 1 shows the specifications for each stent used in this study. All stent models share the same diameter of 3.05 mm and wall thickness of 0.13 mm, ensuring a consistent radial dimension across the configurations. However, the stent length was varied across the models (Model 2 to Model 6) to systematically investigate the influence of landing zone coverage on intra-aneurysmal hemodynamics. Model 2 represents the minimum functional length required to cover the aneurysm neck. Models 3 through 6 represent incrementally longer devices, extending the proximal and distal landing zones within the parent artery. This variation allows for the assessment of how the length of flow straightening upstream of the aneurysm affects the diversion efficiency and whether extended coverage provides superior reduction in the aneurysmal inflow jet [8], [24].

Table 1 *Specification for each stent*

Type of stent	Diameter (mm)	Length (mm)	Thickness
Type 1	3.05	18.20	0.13
Type 2	3.05	17.05	0.13
Type 3	3.05	15.05	0.13
Type 4	3.05	15.90	0.13
Type 5	3.05	15.90	0.13

2.4 Meshing of Stented Intracranial Aneurysms Model

The computational domains were discretised using unstructured tetrahedral elements to accurately capture the intricate arterial geometry and the explicit substructure of the flow diverter stents. This approach was selected to resolve complex hemodynamic features, including velocity gradients and wall shear stress in critical regions [26]. The meshing strategy prioritized solution accuracy, with curvature-based refinement applied in regions of high geometric complexity, particularly around the aneurysm neck and the stent struts.

Across the six configurations, the mesh density was optimized to ensure grid independence and capture the boundary layer flow. Model 1 employed 371,180 nodes and 1,194,212 elements with a fine element size of 0.13 mm, enabling precise representation of stent features. For the stented configurations (Models 2-6), the presence of the stent struts required further local refinement to resolve the flow separation around the wires. By contrast, Model 2 used the coarsest mesh, consisting of 1,462,869 nodes and 4,876,818 elements at an element size of 3.05 mm, which provided adequate resolution of global flow patterns while reducing computational demand. For instance, Model 2, which featured a dense stent configuration, comprised 4.8 million elements with a global maximum size of 0.20 mm and refined sizing of approximately 0.02 mm near the stent wires to capture the micro-flow dynamics. The variation in node counts across models reflects the geometric differences in stent coverage rather than inconsistent meshing standards. Model 3 was constructed with 424,516 nodes and 1,406,535 elements at an element size of 2.50 mm, while Model 4 utilized 342,721 nodes and 1,131,613 elements with a smaller element size of 1.75 mm to improve accuracy in regions of higher curvature. Likewise, Model 5 contained 353,377 nodes and 1,872,135 elements at an element size of 2.50 mm, and Model 6 comprised 931,676 nodes and 3,077,746 elements with the same element size of 2.50 mm, offering refined resolution suitable for hemodynamic evaluation [27].

The final computational mesh exhibited high quality, with an average skewness of 0.28115 and an orthogonal quality of 0.97285. These metrics surpass the recommended criteria for cardiovascular simulations in ANSYS Fluent. As shown in Fig. 4(a), the mesh transitions smoothly from the core flow to the wall boundaries. To accurately resolve the near-wall velocity gradients, inflation layers were generated with five boundary layers along the arterial wall and stent surfaces, as depicted in Fig. 4(b). Furthermore, Fig. 4(b) illustrates the detailed mesh refinement around the stent struts, ensuring precise detection of low-shear zones associated with thrombosis risk [25].

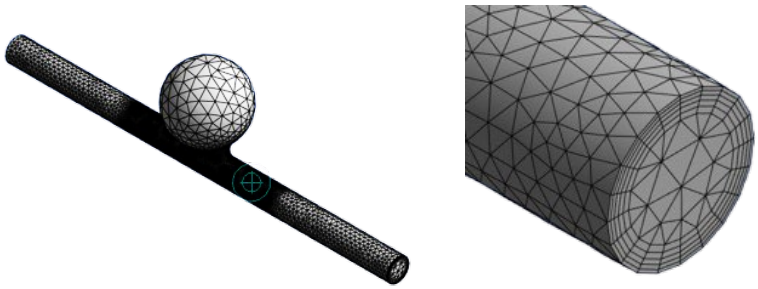

(a) **(b)**

Fig. 4 *Tetrahedral meshing for all intracranial artery over all the stents (a) Body sizing; (b) Inflation*

2.5 Boundary Conditions and Parameter Assumptions

The present numerical study simulated the hemodynamic behaviour within a stented intracranial artery segment by assuming transient, incompressible flow conditions. The flow regime was considered laminar, justified by the low Reynolds number (Re) typically observed in arteries of this anatomical scale, which remains below the critical threshold for turbulence. To ensure a physiologically relevant representation, blood was modelled with a constant density (ρ) of 1055 kg/m^3. Although blood exhibits non-Newtonian characteristics, its rheological properties were simplified in this study by applying a constant dynamic viscosity (μ) of 0.004 Pa·s [23].

The inlet boundary condition was defined using a time-dependent pulsatile velocity profile to represent pulsatile flow within the intracranial artery. This approach captures the physiological time-dependent variation of blood velocity induced by the cardiac cycle in a rigid, cylindrical vessel. The solution accounts for both fluid viscosity and pulsation frequency, yielding a velocity distribution that varies in magnitude and radial shape throughout the cycle. To approximate the cardiac cycle, a simplified sinusoidal waveform was applied. Fig. 5 illustrates the temporal variation of the inlet condition, represented by a simplified sinusoidal waveform over two cardiac cycles 2 s. For the transient simulation of the pulsatile blood flow, a fixed step size of 0.02 s was utilized to resolve the temporal variations across the cardiac cycle. To ensure numerical stability and convergence of the

solution, the solver was configured to perform a minimum of 5 iterations per time step before advancing to the next time level. The velocity fluctuates between a diastolic minimum of approximately 0.18 m/s and a systolic maximum of nearly 0.30 m/s, with a mean time-averaged value of 0.25 m/s [28].

The arterial walls and stent surfaces were subjected to no-slip boundary conditions, thereby imposing zero velocity at the fluid–solid boundaries. Gravitational effects were considered negligible in comparison with the prescribed inlet velocity and outlet pressure [17]. Under these assumptions, the computational setup provides a physiologically consistent representation of steady laminar blood flow assist within the intracranial artery, allowing detailed assessment of velocity fields, pressure distributions, and wall shear stress (WSS) patterns associated with the presence of the stent. To resolve the pressure–velocity coupling, the coupled algorithm in ANSYS Fluent was implemented, which simultaneously updates both variables during each iteration. This numerical approach was adopted to ensure robust convergence and to enhance the accuracy of the predicted hemodynamic environment and WSS characteristics in the stented intracranial artery [19], [25].

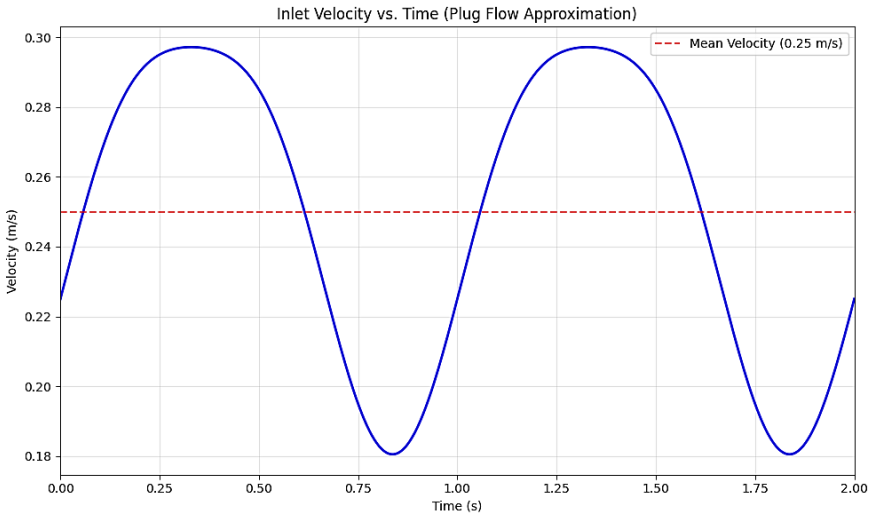

Fig. 5 *Sinusoidal inlet velocity profile with a mean of 0.25 m/s*

2.5.1 Grid Independence Test

Ensuring that the computational fluid dynamics (CFD) simulation results were independent of mesh density required conducting a Grid Independence Test (GIT) for the Type 3 stent in Model 4. This validation step was essential to confirm the accuracy and robustness of the numerical model [29]. The test involved systematic mesh refinement, as outlined in Table 2, where five different configurations were examined. The mesh density ranged from a coarse setup GIT 1 with approximately 716,000 elements to a fine mesh GIT 5 exceeding 1.2 million elements. The objective was to determine the mesh resolution capable of producing stable results while maintaining computational efficiency [30].

The velocity profiles obtained from these configurations are illustrated in Fig. 6, showing a consistent convergence pattern. While the course meshes GIT 1 and GIT 2 produced noticeable variations, the profile generated by GIT 3 closely matched those of the finer meshes GIT 4 and GIT 5. This demonstrated that grid independence was achieved at the GIT 3 level, as the difference in WSS between GIT 3 and the denser meshes remained below 1.5%. Hence, the GIT 3 configuration was selected as the most suitable option, providing a balance between solution accuracy and computational cost [31].

Table 2 *Parameter used in GIT for model 3*

Parameter	GIT 1	GIT 2	GIT 3	GIT 4	GIT 5
Element size	4.00 mm	3.50 mm	3.05 mm	1.75 mm	0.30 mm
Number of nodes	223134	249131	280105	342721	374981
Number of elements	715927	809353	916877	1131613	1226306

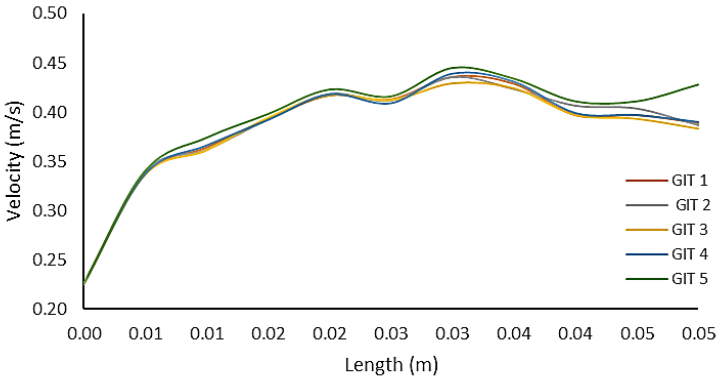

Fig. 6 *GIT chart for Type 3 stent configuration in simplified model*

3. Results

This section presents the findings of the computational analysis conducted to investigate the hemodynamic behavior of blood flow within intracranial aneurysms treated using different stent designs and deployment strategies.

3.1 Velocity Profile of Intracranial Aneurysms Model

The investigation into the haemodynamic environment of intracranial aneurysms, as depicted in Fig. 7, reveals significant variations in intra-aneurysmal velocity contingent upon the deployed stent model. Model 1, the control case without a stent, establishes a baseline for an untreated aneurysm. In this configuration, a high-velocity jet with a core velocity of approximately 0.39 ± 0.04 m s^{-1} directly impinges upon the aneurysm sac. This ingress of rapid flow induces a large, stable vortex within the sac, maintaining significant fluid motion and potentially contributing to wall shear stress and growth. The velocity at the neck and within the upper region of the aneurysm sac remains elevated, ranging from 0.22 to 0.35 m s^{-1}, indicating a high risk of continued haemodynamic stress on the weakened vessel wall. This model represents the pathological condition that necessitates intervention to mitigate the risk of rupture [32].

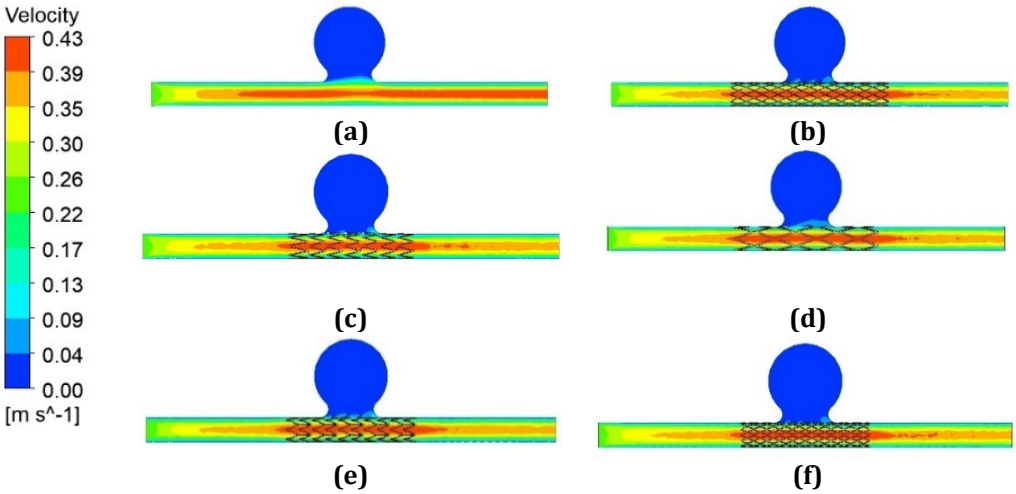

Fig. 7 *Vector velocity for the six model of intracranial aneurysms (a) Model 1; (b) Model 2; (c) Model 3; (d) Model 4; (e) Model 5; (f) Model 6*

A comparative evaluation of the stented configurations Model 2 until 6 reveals a distinct relationship between stent geometry and flow-diverting efficiency. Models 2 and 5 achieve a moderate yet significant decrease in intra-aneurysmal velocity. The stents in these models effectively disrupt the primary inflow jet, lowering the velocity within the aneurysm sac to approximately 0.09-0.17 m s^{-1} — representing a 55-75% reduction relative to the untreated case. Despite this improvement, a residual, slower circulation pattern remains observable. Conversely, Models 3 and 4 demonstrate superior flow diversion, reducing intra-aneurysmal velocity further to 0.04-0.09 m s^{-1}. This pronounced reduction fosters a near-stagnant flow condition, which is favorable for thrombosis initiation [33].

Among the analysed configurations, Model 6 is identified as the most efficient in diverting blood flow. This model achieves an almost complete flow stagnation within the aneurysm sac, where velocities are consistently reduced to the range of 0.00-0.04 m s^{-1}. This corresponds to a reduction exceeding 90% compared to the untreated baseline on Model 1. The markedly low velocity indicates that the stent effectively isolates the aneurysm from the main circulatory flow and pressure, establishing a haemodynamic condition that favours thrombus formation and promotes long-term stable occlusion [34]. The progressive enhancement observed from Model 2 to Model 6 highlights the importance of stent design parameters particularly strut density and porosity in optimising flow diversion and improving potential clinical outcomes [35].

3.2 Wall Shear Stress Distribution at Intracranial Aneurysms Model

The comparative analysis highlights the influence of different stent configurations on wall shear stress (WSS) distribution within an intracranial aneurysm. Fig. 7 illustrates the WSS contours for each model, enabling a clear visualization of the hemodynamic variations induced by stent deployment. The untreated aneurysm, represented by Model 1, serves as the baseline, exhibiting a hemodynamic environment with elevated WSS, particularly at the aneurysm neck on the distal side where the blood jet impinges. This impingement region shows peak WSS values ranging from 4.70 to 5.00 Pa, signifying a high-risk zone for aneurysm growth or rupture [7]. In contrast, the WSS within the aneurysm sac is lower and more irregular, approximately between 2.30 and 3.50 Pa, suggesting a disturbed flow structure. Meanwhile, the parent artery maintains a nearly uniform WSS of about 3.80 ± 0.30 Pa, serving as a reference for normal hemodynamic behavior [16], [33].

The application of stents, as demonstrated in Models 2 through 6, markedly alters the intra-aneurysmal hemodynamic, producing a beneficial flow diversion effect. The previously concentrated high WSS at the aneurysm neck is eliminated, resulting in a consistent low WSS distribution across the aneurysm sac, ranging from 2.00 to 2.30 Pa. This uniform reduction reflects effective flow diversion, as the stents redirect the high-velocity jet away from the aneurysm, inducing a quasi-static flow condition. Clinically, this low WSS environment is desirable, as it facilitates thrombus formation and promotes aneurysm healing by minimizing stress on the aneurysm wall [36].

Although all stented models achieve a similar overall reduction in intra-aneurysmal WSS, subtle differences appear along the parent artery wall where stents are deployed. Models 2, 3, and 5 produce moderately uniform WSS distributions, typically between 2.90 and 3.80 Pa, reflecting simpler stent geometries. In contrast, Model 4 generates a more complex WSS profile due to a denser or overlapping mesh design, resulting in localized WSS peaks around 4.10 Pa, which indicates regions of intensified flow interaction near the struts. Model 6 closely resembles Model 5, implying comparable porosity or geometric characteristics. Overall, all stent designs demonstrate strong flow-diverting capability, effectively lowering WSS within the aneurysm sac to therapeutic levels while maintaining acceptable local variations along the stented vessel segment [37].

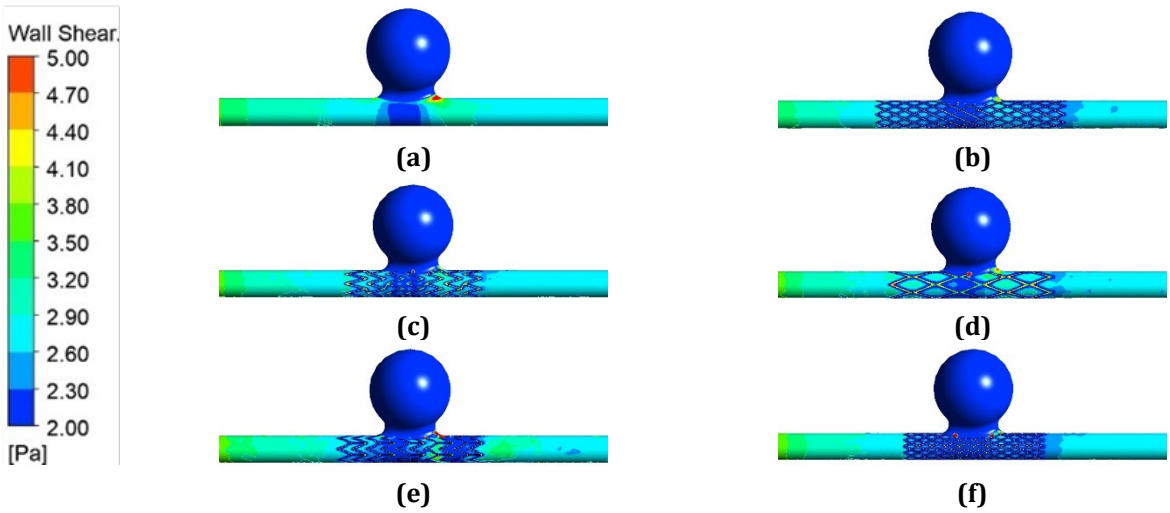

Fig. 8 *Wall shear stress distribution for the six model of intracranial aneurysms (a) Model 1; (b) Model 2; (c) Model 3; (d) Model 4; (e) Model 5; (f) Model 6*

Table 3 quantitatively summarizes the area-weighted average wall shear stress (WSS) for each model, providing an integrated measure of overall haemodynamic behavior. Models 1 and 2 serve as the baseline, with WSS values of 2.0596 Pa and 2.0673 Pa, respectively. Model 3 records the lowest WSS at 1.9456 Pa, reflecting a 5.54% reduction compared to Model 1. Likewise, Model 4 demonstrates a decrease to 1.9593 Pa, equivalent to a

4.87% drop from the baseline. Conversely, Model 5 produces the highest WSS at 2.1167 Pa—an increase of 2.77% relative to Model 1—while Model 6 yields a slightly lower value of 2.0140 Pa, representing a 2.21% reduction. Overall, the WSS variation across models remains confined within approximately ±5.6%, indicating that although local WSS distributions undergo substantial modification due to differing stent configurations, the averaged WSS remains relatively consistent [38]. The elevated WSS observed in Model 5, despite pronounced visual flow diversion, implies that its stent design may generate localized high-velocity jets that increase shear stress at specific wall regions, an effect that becomes averaged within the global WSS metric [25].

The area-weighted average wall shear stress (WSS) varies minimally among the different models for intracranial aneurysm treatment—by approximately 0.2 Pa or within a ±5.6% range—these seemingly small differences have significant physiological implications. Stent configurations that result in lower WSS, such as Model 3 (5.54% reduction), may heighten the risk of adverse events like endothelial dysfunction, neointimal formation, and thrombosis. Conversely, the design in Model 5, which produced the highest WSS (2.77% increase), can generate localized high-velocity jets. Such accelerated flow patterns can induce localized areas of high shear stress, particularly around stent struts, potentially causing platelet activation or endothelial damage. These findings highlight the critical role of stent geometry and placement in modulating the WSS distribution, underscoring the necessity of meticulous design to optimize hemodynamic performance and ensure long-term vascular health [18].

Table 3 *Area-weighted average wall shear stress (Pa) for each model*

Type of model	Area-average wall shear stress (Pa)
Model 1	2.0596
Model 2	2.0673
Model 3	1.9456
Model 4	1.9593
Model 5	2.1167
Model 6	2.0140

3.3 Pressure Distribution at Intracranial Aneurysms Model

The pressure distribution across the six computational models, as illustrated in Fig. 9, clearly reflects the significant hemodynamic influence of stent deployment in altering intra-aneurysmal pressure. In the baseline condition represented by Model 1, the aneurysm sac exhibits consistently high pressure that remains continuous with the parent artery, with values predominantly ranging from 206.03 Pa to 235.46 Pa, as shown by the yellow to light-orange regions. This sustained high-pressure state substantially contributes to wall stress development and elevates the risk of aneurysm rupture. In contrast, Models 2 to 6 display varying degrees of pressure mitigation depending on the stent configuration, highlighting the role of design parameters in influencing hemodynamic performance [13], [39]. A consistent trend is observed, where stent placement at the aneurysm neck progressively decreases intra-sac pressure by redirecting blood flow along the main vessel axis [39].

Furthermore, Models 2 and 3 demonstrate moderate but noticeable reductions, with pressure values decreasing to approximately 147.16-176.59 Pa, indicating a 30-40% reduction relative to the baseline model. Model 4 exhibits a more significant improvement, with pressure values reduced to between 58.86 Pa and 88.30 Pa, corresponding to a reduction exceeding 65%. The most pronounced reduction is evident in Models 5 and 6, which exhibit superior flow-diverting capabilities and enhanced pressure attenuation. Model 5 records an average pressure of about 58.86 ± 29.43 Pa, while Model 6 achieves the greatest reduction, where most regions within the aneurysm sac experience pressures below 29.43 Pa. This corresponds to a remarkable decrease exceeding 90% compared to the untreated case, effectively isolating the aneurysm from major hemodynamic forces. The progressive decline in pressure from Model 2 through Model 6 clearly indicates that increasing the stent mesh density enhances the flow-diversion effect, resulting in a stable, low-pressure environment that promotes thrombus formation and supports aneurysm stabilization [33].

Int. Journal of Integrated Engineering Vol. 17 No. 8 (2025) p. 285-300

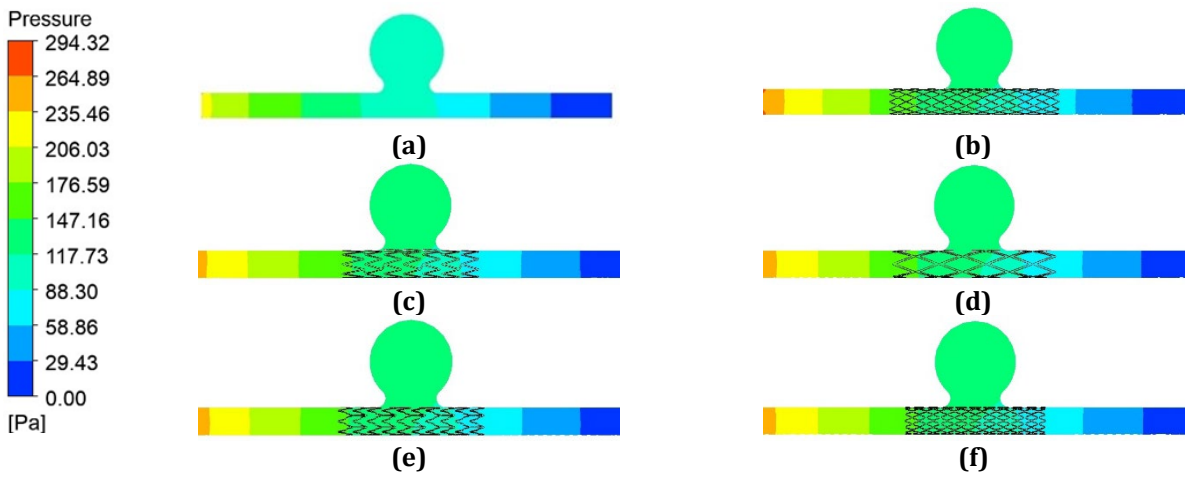

Fig. 9 *Pressure distribution for the six model of intracranial aneurysms (a) Model 1; (b) Model 2; (c) Model 3; (d) Model 4; (e) Model 5; (f) Model 6*

Based on the data presented in Table 4, the analysis of pressure distribution reveals clear variations among the six stent models, reflecting distinct hemodynamic responses to differences in design and implantation configuration. The overall pressure range recorded across all models was 6.38 Pa, indicating measurable differences in performance. Model 1 displayed the highest-pressure distribution with a value of 102.14 Pa, while Model 5 recorded the lowest at 95.76 Pa. When Model 2, with a mean pressure of 100.00 Pa, is considered as the reference baseline, Model 1 is the only configuration that shows an increase in pressure. In contrast, the remaining models—Model 3, Model 4, Model 5, and Model 6—exhibit reduced pressure values of 97.54 Pa, 97.98 Pa, 95.76 Pa, and 96.24 Pa respectively. Among these, Model 5 demonstrates the most pronounced reduction, followed closely by Model 6. These observations indicate that the geometric designs of Model 5 and Model 6 are more effective in minimising localized pressure concentrations compared to the other configurations, particularly Model 1, which exhibits the least favourable pressure characteristics [32].

Table 4 *Pressure distribution across stent designs and implantation positions*

Type of model	Pressure distribution (Pa)
Model 1	102.14
Model 2	100.00
Model 3	97.54
Model 4	97.98
Model 5	95.76
Model 6	96.24

3.4 Impact of the Stents on the WSS-Related Indices: OSI

The spatial distribution of the Oscillatory Shear Index (OSI) across the six computational aneurysm models, as depicted in Fig. 10, reveals clear hemodynamic differences resulting from the various intervention strategies applied. In the baseline condition represented by Model 1, the OSI remains uniformly low, with values close to zero throughout the parent vessel and the aneurysm sac. This indicates a reference flow condition that, while complex, exhibits minimal oscillatory behaviour. Similarly, Model 2, incorporating a conventional stent positioned across the aneurysm neck, shows only a negligible change in OSI compared to the baseline, suggesting that this configuration exerts minimal influence on flow oscillation within the aneurysm region [21].

In contrast, the introduction of flow-diverting stents in Models 3 through 6 produces markedly different hemodynamic responses. Models 3, 4, and 6 display a slight increase in OSI, primarily concentrated around the aneurysm neck, with values ranging from approximately 0.10 to 0.15, while the OSI within the aneurysm sac remains relatively low. This trend implies that these configurations effectively stabilise intra-aneurysmal flow and promote favourable flow diversion [23]. However, Model 5 demonstrates a notably adverse hemodynamic condition, where a large portion of the aneurysm sac experiences OSI values between 0.40 and 0.50—representing an increase exceeding 200% compared to the other flow diverter models. This elevated OSI indicates highly unstable, reversing flow patterns that are detrimental to vascular stability [40].

The interpretation of these OSI variations is closely associated with the Time-Averaged Wall Shear Stress (WSS). A high OSI value generally corresponds to low WSS, and an OSI approaching 0.5 signifies a near-zero mean shear stress, where the flow direction reverses during roughly half of the cardiac cycle [7]. For Models 3, 4, and 6, the combination of low OSI within the aneurysm sac and effective flow diversion encourages blood stasis and thrombus formation, which aligns with the intended therapeutic outcome. Conversely, the abnormally high OSI observed in Model 5 indicates an unfavourable hemodynamic environment that may induce endothelial dysfunction and inhibit stable thrombosis, thereby increasing the likelihood of treatment failure and potential aneurysm instability [35].

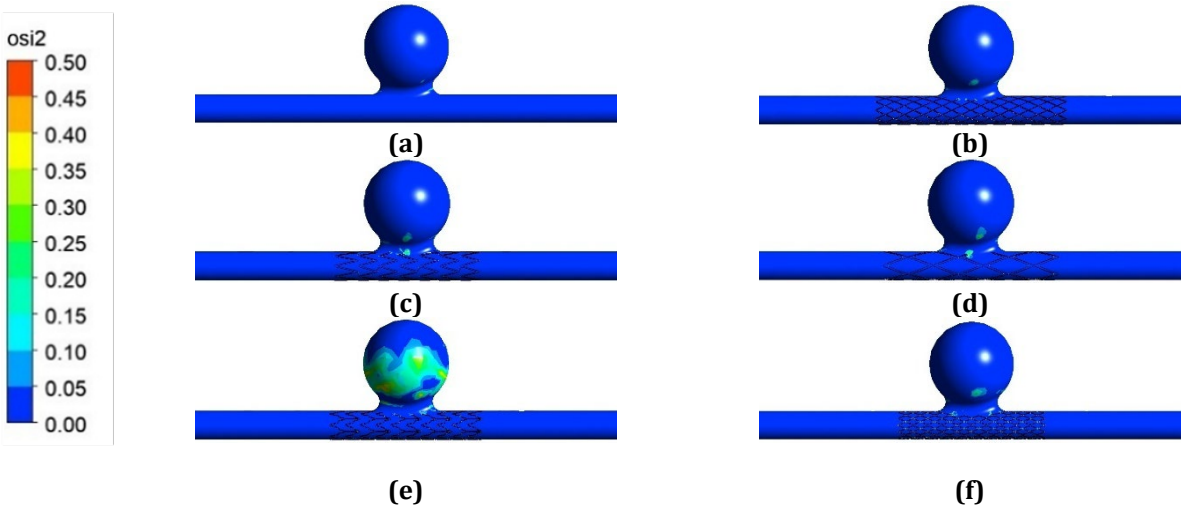

Fig. 10 *Spatial configuration of oscillatory shear index (OSI) for the six model of intracranial aneurysms (a) Model 1; (b) Model 2; (c) Model 3; (d) Model 4; (e) Model 5; (f) Model 6*

3.5 Impact of the Stents on the WSS-Related Indices: RRT

The spatial variation of Relative Residence Time (RRT), a key hemodynamic parameter linked to blood stasis, is illustrated in Fig. 11 for six computational models of intracranial aneurysms. In the baseline configuration represented by Model 1, which depicts the untreated condition, a non-uniform RRT pattern is observed within the aneurysm sac. The parent artery records an RRT value close to 0.00 Pa^{-1}, indicating normal and healthy blood flow. In contrast, the aneurysm sac demonstrates a highly elevated RRT region, reaching approximately 300 Pa^{-1}, signifying significant flow recirculation and prolonged residence time at the apex. This condition is commonly linked to aneurysm enlargement and rupture risk [23]. The remaining areas of the sac exhibit moderate RRT values between 150 and 240 Pa^{-1}, reflecting a complex and irregular intra-aneurysmal flow environment [41].

Following the placement of flow-diverting stents, noticeable hemodynamic modifications can be observed across the treated models. Models 2, 3, and 6 display the most favourable therapeutic responses, where the RRT distribution becomes uniformly elevated to around 300 Pa^{-1} across almost the entire aneurysm sac. This outcome represents a substantial improvement compared to the untreated baseline, effectively transforming the aneurysm cavity into a region of near-total blood stasis—an essential condition for promoting thrombosis and facilitating aneurysm occlusion [8]. Model 4 also demonstrates a beneficial effect, with a broad area of elevated RRT throughout most of the sac. However, a small region near the aneurysm neck maintains relatively lower RRT values ranging between 180 and 210 Pa^{-1}, suggesting that its flow diversion efficiency is slightly less comprehensive than that of Models 2, 3, and 6. The overall area exhibiting optimal blood stasis in Model 4 is estimated to be about 10–15% smaller than that observed in Model 6 [11].

In contrast, Model 5 presents a markedly adverse hemodynamic outcome. Instead of promoting blood stasis, this configuration results in a pronounced decrease in RRT within the aneurysm sac, with values dropping to nearly zero, ranging between 0 and 30 Pa^{-1}. This reduction is considerably lower than that observed in the untreated model, indicating that the stent has failed to induce flow stagnation and may have inadvertently caused a washout effect [12]. Such a condition increases the mechanical stress exerted on the aneurysm wall and counteracts the intended therapeutic objective. The mean RRT in Model 5 is approximately 90–95% lower than the effective RRT levels recorded in Model 6. These findings highlight that the therapeutic performance of flow diverters is highly dependent on their geometric configuration and positioning. Overall, Models 2, 3, and 6 demonstrate strong potential in achieving effective intra-aneurysmal stasis conducive to thrombosis and eventual occlusion, whereas Model 5 produces a hemodynamically unfavourable response that could compromise treatment success [2].

Int. Journal of Integrated Engineering Vol. 17 No. 8 (2025) p. 285-300

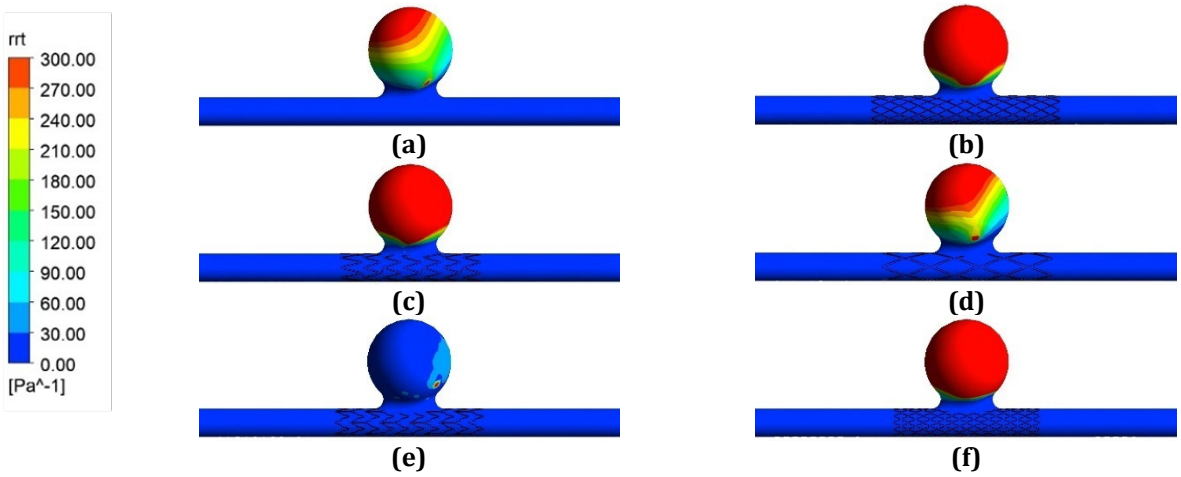

Fig. 11 *Spatial configuration of relative residence time (RRT) for the six model of intracranial aneurysms (a) Model 1; (b) Model 2; (c) Model 3; (d) Model 4; (e) Model 5; (f) Model 6*

4. Conclusions

Based on the comprehensive computational fluid dynamics (CFD) analysis, the hemodynamic environment within an intracranial aneurysm is strongly influenced by the geometric configuration and deployment characteristics of flow-diverting stents. Among the evaluated models, Model 6 exhibited the most effective therapeutic performance by achieving near-complete flow stagnation, with velocity and pressure reductions exceeding 90% compared to the untreated baseline at Model 1, thereby effectively isolating the aneurysm sac from direct hemodynamic impact. All stented models successfully reduced intra-aneurysmal wall shear stress (WSS) to levels conducive to thrombosis formation; however, Models 6, 2, and 3 demonstrated the most favorable intra-aneurysmal stasis, as indicated by uniformly elevated Relative Residence Time (RRT). Conversely, Model 5 showed suboptimal hemodynamic behavior, characterized by an abnormally high Oscillatory Shear Index (OSI) and a counterproductive reduction in RRT, which may compromise thrombus stability and increase the risk of treatment failure. Overall, the findings underscore the critical importance of stent design—particularly mesh density—in regulating intra-aneurysmal flow dynamics to establish a low-flow, low-pressure environment that promotes thrombosis and ensures long-term aneurysm occlusion stability.

Acknowledgement

This research was supported by the Ministry of Higher Education (MOHE) through the Fundamental Research Grant Scheme (FRGS/1/2024/TK10/UTHM/02/6), Vot K514.

Conflict of Interest

The authors declare that there is no conflict of interest regarding the publication of the paper.

Author Contribution

The authors confirm contribution to the paper as follows: ***study conception and design:*** *Muhammad Affiq Syukri Arafat, Ishkrizat Taib, Nor Adrian Nor Salim, Mohd Syahar Mohd Shawal, Mohd Rosdzimin Abdul Rahman;* ***data collection:*** *, Muhammad Affiq Syukri Arafat, Ishkrizat Taib, Nor Adrian Nor Salim, Mohd Syahar Mohd Shawal, Mohd Rosdzimin Abdul Rahman;* ***analysis and interpretation of results:*** *Muhammad Affiq Syukri Arafat;* ***draft manuscript preparation:*** *Muhammad Affiq Syukri Arafat, Nur Amani Hanis Roseman. All authors reviewed the results and approved the final version of the manuscript.*

References

[1] H. Zhang, L. Li, F. Miao, J. Yu, B. Zhou & Y. Pan (2022) Computational fluid dynamics analysis of intracranial aneurysms treated with flow diverters: A case report, *Neurochirurgie*, *68(2)*, 235-238. https://doi.org/10.1016/j.neuchi.2021.03.007

[2] Pablo Jeken Rico (2024). *Hemodynamic Modelling and Simulation of Flow Diverters for Intracranial Aneurysm Treatment* (Doctoral dissertation, Université Paris sciences et lettres).

[3] Jingfeng Luo, Yuxuan Luo, Jihong Sun, Yurong Zhou, Yajing Zhang &Xiaoming Yang (2015) Adeno-associated virus-mediated cancer gene therapy: Current status, *Cancer letters*, *356(2)*, 347-356, https://doi.org/10.1016/j.canlet.2014.10.045

[4] Dong-Seong Shin, Christopher P. Carroll, Mohammed Elghareeb, Brian L. Hoh & Bum-Tae Kim (2020) The evolution of flow-diverting stents for cerebral aneurysms; historical review, modern application, complications, and future direction, *Journal of Korean Neurosurgical Society*, *63(2)*, 137-152, https://doi.org/10.3340/jkns.2020.0034

[5] Michael Gaub, Greg Murtha, Molly Lafuente, Matthew Webb, Anqi Luo, Lee A. Birnbaum, Justin R. Mascitelli & Fadi Al Saiegh (2024), Flow diversion for endovascular treatment of intracranial aneurysms: past, present, and future directions, *Journal of Clinical Medicine*, *13(14)*, 4167, https://doi.org/10.3390/jcm13144167

[6] Paulo R Cillo-Velasco, Rafaello D. Luciano, Michael E. Kelly, Lissa Peeling, Donald J. Bergstrom, Xiongbiao Chen & Mauro Malvè (2020). The hemodynamics of aneurysms treated with flow-diverting stents considering both stent and aneurysm/artery geometries, *Applied Sciences*, *10(15),* 5239, https://doi.org/10.3390/app10155239

[7] H. Meng, V. M. Tutino, J. Xiang & Ajajon Siddiqui (2014) High WSS or low WSS? Complex interactions of hemodynamics with intracranial aneurysm initiation, growth, and rupture: toward a unifying hypothesis, *American Journal of Neuroradiology*, *35(7)*, 1254-1262, https://doi.org/10.3174/ajnr.A3558

[8] Zbigniew Tyfa, Karol Wiśniewski, Piotr Reorowicz & Krzysztof Jóźwik (2025) Blood flow simulations in a cerebral aneurysm secured by a Flow Diverter stent, *Acta of Bioengineering & Biomechanics*, *27(2)*. https://doi.org/10.37190/abb/205428

[9] Chivukula, Venkat Keshav, Michael R. Levitt, Alicia Clark, Michael C. Barbour, Kurt Sansom, Luke Johnson, Cory M. Kelly, Christian Geindreau, Sabine Rolland du Roscoat, Louis J. Kim & Alberto Aliseda (2019) Reconstructing patient-specific cerebral aneurysm vasculature for in vitro investigations and treatment efficacy assessments, *Journal of Clinical Neuroscience*, *61*, 153-159, https://doi.org/10.1016/j.jocn.2018.10.103

[10] Sima Baheri Islami, Mike Wesolowski, William Revell & Xiongbiao Chen (2021) Virtual reality visualization of CFD simulated blood flow in cerebral aneurysms treated with flow diverter stents, *Applied Sciences*, *11(17)*, 8082, https://doi.org/10.3390/app11178082

[11] Chong, Winston, Yu Zhang, Yi Qian, Leontat Lai, G. Parker & K. Mitchell (2014) Computational hemodynamics analysis of intracranial aneurysms treated with flow diverters: correlation with clinical outcomes, *American Journal of Neuroradiology*, *35(1)*, 136-142, https://doi.org/10.3174/ajnr.A3790

[12] Maria Antonietta Boniforti, Roberto Magini & Tania Orosco Salinas. (2023) Hemodynamic investigation of the flow diverter treatment of intracranial aneurysm, *Fluids*, *8(7)*, 189, https://doi.org/10.3390/fluids8070189

[13] Yu Liu, Shuang Li, Haipeng Liu, Xuan Tian, Yuying Liu, Ziqi Li, Thomas W. Leung & Xinyi Leng (2025) Clinical implications of haemodynamics in symptomatic intracranial atherosclerotic stenosis by computational fluid dynamics modelling: a systematic review, *Stroke and Vascular Neurology*, *10(1)*, e003202, https://doi.org/10.1136/svn-2024-003202

[14] Prantik Roy Chowdhury, Victor K. Lai & Ruihang Zhang (2025). Flow Dynamics in Brain Aneurysms: A Review of Computational and Experimental Studies, *Biomechanics*, *5(2)*, 36, https://doi.org/10.3390/biomechanics5020036

[15] Yi-Ze Li, Sheng-Nan Kong, Yun-Peng Liu, Yue Yang & Hong-Mei Zhang (2023) Can liquid biopsy based on ctDNA/cfDNA replace tissue biopsy for the precision treatment of EGFR-mutated NSCLC? *Journal of Clinical Medicine*, *12*(4), 1438, https://doi.org/10.3390/jcm12041438

[16] Yasuyuki Umeda, Fujimaro Ishida, Masanori Tsuji, Kazuhiro Furukawa, Masato Shiba, Ryuta Yasuda, Naoki Toma, Hiroshi Sakaida & Hidenori Suzuki (2017) Computational fluid dynamics (CFD) using porous media modeling predicts recurrence after coiling of cerebral aneurysms, *PloS One*, *12(12)*, e0190222, https://doi.org/10.1371/journal.pone.0190222

[17] Burcu Ramazanli, Oyku Yagmur, Efe Cesur Sarioglu & Huseyin Enes Salman (2025) Modeling techniques and boundary conditions in abdominal aortic aneurysm analysis: Latest developments in simulation and integration of machine learning and data-driven approaches, *Bioengineering*, *12(5)*, 437, https://doi.org/10.3390/bioengineering12050437

[18] Haveena Anbananthan, Phani Kumari Paritala, Jessica Benitez Mendieta, Han Yu, Tiago Guerzet Sardenberg Lima, Zoe Dettrick, Ee Shern Liang, Alan Coulthard, Zhi-Yong Li & Craig Winter (2025) Haemodynamic characteristics of thin-walled regions in intracranial aneurysms: intraoperative imaging and CFD analysis, *Acta Neurochirurgica*, *167(1)*, 238, https://doi.org/10.1007/s00701-025-06660-y

[19] Borja Catalán-Echeverría, Michael E. Kelly, Lissa Peeling, Donald Bergstrom, Xiongbiao Chen & Mauro Malvè (2019) CFD-based comparison study of a new flow diverting stent and commercially-available ones for the treatment of cerebral aneurysms, *Applied Sciences*, *9(7)*, 1341, https://doi.org/10.3390/app9071341

[20] Hanie Asgari (2022) *Numerical simulations of bifurcation cerebral aneurysm hemodynamics* (Doctoral dissertation, University of British Columbia). https://doi.org/10.14288/1.0412757

[21] Muhammad Sufyan Amir Paisal, Ishkrizat Taib, Ahmad Mubarak Tajul Arifin & Muhammad Faisal Mahmod (2019) Evaluation system on haemodynamic parameters for stented carotid artery: Stent pictorial selection method, *International Journal of Integrated Engineering*, *11(1)*, 225-246, https://doi.org/10.30880/ijie.2019.11.01.024

[22] Lim Sheh Hong, Mohd Azrul Hisham Mohd Adib, Muhammad Uzair Matalif, Mohd Shafie Abdullah, Nur Hartini Mohd Taib & Radhiana Hassan (2020, September), Modeling and simulation of blood flow analysis on simplified aneurysm models, In *IOP Conference Series: Materials Science and Engineering, 917(1)*, 012067. IOP Publishing. https://doi.org/10.1088/1757-899X/917/1/012067

[23] Sunghan Kim, Hyeondong Yang, Ineui Hong, Je Hoon Oh & Yong Bae Kim (2021) Computational study of hemodynamic changes induced by overlapping and compacting of stents and flow diverter in cerebral aneurysms, *Frontiers in Neurology*, *12*, 705841, https://doi.org/10.3389/fneur.2021.705841

[24] Chen Pan, Yafeng Han & Jiping Lu (2021), Structural design of vascular stents: A review, *Micromachines*, *12(7)*, 770, https://doi.org/10.3390/mi12070770

[25] Che Mohammad Hafizal Muzammil Che Seman, Nur Ayuni Marzuki, Nofrizalidris Darlis, Noraini Marsi, Zuliazura Mohd Salleh, Izuan Amin Ishak, Ishkrizat Taib & Safra Liyana Sukiman (2020) Comparison of hemodynamic performances between commercial available stents design on stenosed femoropopliteal artery, *CFD Letters*, *12*(7), 17-25, https://doi.org/10.37934/cfdl.12.7.1725

[26] M. A. Castro, Christopher M. Putman & J. R. Cebral (2006) Computational fluid dynamics modeling of intracranial aneurysms: effects of parent artery segmentation on intra-aneurysmal hemodynamics, *American Journal of Neuroradiology*, *27(8)*, 1703-1709,

[27] Nur Farahalya Razhali & Ishkrizat Taib (2022) Analysis of hemodynamic on different stent strut configurations in femoral popliteal artery, *CFD Letters*, *14(3)*, 119-128, https://doi.org/10.37934/cfdl.14.3.119128

[28] Benjamin Csippa, Levente Sándor, Gábor Závodszky, István Szikora & György Paál (2024) Comparison of flow reduction efficacy of nominal and oversized flow diverters using a novel measurement-assisted in silico method, *Clinical Neuroradiology*, *34(3)*, 675-684, https://doi.org/10.1007/s00062-024-01404-4

[29] Arul Nalmanan Raja Gopal (2025) Comparative study of internal flow dynamics using CFD for of sudden expansion pipe, *Journal of Advances in Fluid, Heat, and Materials Engineering*, *5(1)*, 37-44, https://doi.org/10.37934/afhme.5.1.3744a

[30] Nur Farahalya Razhali, Ishkrizat Taib, Nurul Fitriah Nasir, Ahmad Mubarak Tajul Arifin, Nor Adrian Nor Salim, Shahrul Azmir Osman, Nofrizal Idris Darlis & A. K. Kareem (2022) Analysis of hemodynamic effect on different stent strut configuration in femoral popliteal artery during the physical and physiological conditions, *Journal of Advanced Research in Applied Sciences and Engineering Technology*, *29*, 223-236, https://doi.org/10.37934/araset.29.1.223236

[31] Khairul Shafaiz Jesni & Ishkrizat Taib (2024) Computational analysis of temperature distributions on the malignant tumour, *Journal of Advances in Fluid, Heat, and Materials Engineering*, *3(1)*, 10-21, https://doi.org/10.37934/afhme.3.1.1021a

[32] Augusto Fava Sanches, Suprosanna Shit, Yigit Özpeynirci & Thomas Liebig (2022) CFD to quantify idealized intra-aneurysmal blood flow in response to regular and flow diverter stent treatment, *Fluids*, *7(8)*, 254, https://doi.org/10.3390/fluids7080254

[33] Jweeg, Mohsen, Emad Qasem Hussein, Farhan Lafta Rashid, and Ali Basem (2024) Investigation of two-way fluid-structure interaction of blood flow at different temperature using CFD, *Journal of Advanced Research in Applied Sciences and Engineering Technology*, *36*, 120-130, https://doi.org/10.37934/araset.36.2.120130

[34] Nabilah Ibrahim, Nik Farhan Nik Fuad & Nur Shazilah Aziz (2014) Study of vessel conditions in different categories of weight for early-stage of deep vein thrombosis (DVT) diagnosis, *International Journal of Integrated Engineering*, *6(3)*, 57-64, https://publisher.uthm.edu.my/ojs/index.php/ijie/article/view/1042/693

[35] Farouk Mezali, Khatir Naima, Saida Benmamar & Abdelkrim Liazid (2023) Study and modeling of the thrombosis of small cerebral aneurysms, with and without flow diverter, by the lattice Boltzmann method, *Computer Methods and Programs in Biomedicine*, *233*, 107456, https://doi.org/10.1016/j.cmpb.2023.107456

[36] Sheh Hong Lim, Mohd Azrul Hisham Mohd Adib, Mohd Shafie Abdullah, Nur Hartini Mohd Taib, Radhiana Hassan & Azian Abd Aziz (2020) Study of extracted geometry effect on patient-specific cerebral aneurysm model with different threshold coefficient (Cthres), *CFD Letters*, *12(10)*, 1-14, https://doi.org/10.37934/cfdl.12.10.114

[37] Muhammad Sufyan Amir Paisal & Ishkrizat Taib, (2017) Computational analysis on stent geometries in carotid artery: A review, In *IOP Conference Series: Materials Science and Engineering*, *165(1)*, 012003. IOP Publishing. https://doi.org/10.1088/1757-899X/165/1/012003

[38] Christoph Roloff & Philipp Berg (2022) Effect of flow diverter stent malposition on intracranial aneurysm hemodynamics—an experimental framework using stereoscopic particle image velocimetry, *PLoS One*, *17(3)*, e0264688, https://doi.org/10.1371/journal.pone.0264688

[39] Ignacio Larrabide, María Laura Aguilar, Hernán G. Morales, Adrianus Johannes Geers, Zsolt Kulcsár, Daniel Rüfenacht & A. F. Frangi (2013) Intra-aneurysmal pressure and flow changes induced by flow diverters: relation to aneurysm size and shape, *American Journal of Neuroradiology*, *34(4)*, 816-822, https://doi.org/10.3174/ajnr.A3288

[40] Yuya Uchiyama, Soichiro Fujimura, Hiroyuki Takao, Takashi Suzuki, Toshihiro Ishibashi, Katharina Otani, Kostadin Karagiozov, Koji Fukudome, Hideki Yamamoto & Yuichi Murayama (2022) Role of patient-specific blood properties in computational fluid dynamics simulation of flow diverter deployed cerebral aneurysms, *Technology and Health Care*, *30(4)*, 839-850. https://doi.org/10.3233/THC-213216

[41] Yunling Long, Hongyu Yu, Zhizheng Zhuo, Ying Zhang, Yang Wang, Xinjian Yang & Haiyun Li (2014) A geometric scaling model for assessing the impact of aneurysm size ratio on hemodynamic characteristics *BioMedical Engineering OnLine*, *13*(1), 17, https://doi.org/10.1186/1475-925X-13-17